American Mineralogist, Volume 90, pages 1827–1834, 2005

Quantum mechanical calculations of trans-vacant and cis-vacant polymorphism in dioctahedral 2:1 phyllosilicates

C. Ignacio Sainz-Díaz,[1,*] Elizabeth Escamilla-Roa,[2] and Alfonso Hernández-Laguna[2]

[1]Instituto Andaluz de Ciencias de la Tierra, Consejo Superior de Investigaciones Científicas (CSIC)/Universidad de Granada, Av. Fuentenueva s/n, 18002, Granada, Spain

[2]Estación Experimental del Zaidín, Consejo Superior de Investigaciones Científicas (CSIC) C/ Profesor Albareda 1, 18008, Granada, Spain.

Abstract

Trans-vacant and cis-vacant polymorphs of smectites and illites were distinguished by studying different cation substitutions in octahedral and tetrahedral sheets and in the interlayer. The standard Kohn-Sham self-consistent density functional method was used in the generalized gradient approximation (GGA) with numerical atomic orbitals as the basis set. The calculations reproduce the differences in the lattice parameters between the cis-vacant and trans-vacant configurations as observed from experimental studies of phyllosilicates. This theoretical approach is a useful tool for predicting crystallographic properties that must be calculated for smectites and illites because they cannot be determined experimentally in these clay minerals, especially the cis-vacant and trans-vacant configurations. The effect of cation substitutions in the octahedral and tetrahedral sheets on various structural features is also presented. The calculated effects are consistent with experimental results. The energy differences between the cis-vacant and trans-vacant polymorphs for a given composition are lower than the energy changes produced by the relative cation distributions in the octahedral sheet. Nevertheless, in the most illitic samples the trans-vacant arrangement is more stable than the cis-vacant form, in accord with experimental studies.

Introduction

The clays represent one of the largest groups of minerals in sediments. The diversity of dioctahedral 2:1 phyllosilicates is related, in part, to isomorphous cation substitution of Al^{3+} by Fe^{3+} and Mg^{2+} in the octahedral sheet, and Si^{4+} by Al^{3+} in the tetrahedral sheet (e.g., illite, beidellite, montmorillonite, nontronite). These cation substitutions may create order-disorder phenomena in the crystal structure of these minerals. In addition, these phyllosilicates are structurally similar and stacking sequences of component layers may also be ordered or disordered. The various structural disorders and the small particle size of the crystals in clays make it difficult to obtain precise experimental structural data by diffraction techniques, especially for smectite group species and for illites. Thus, the atomic positions in the crystal structures of these minerals have not been reported from experimental data, but they have been extrapolated (Tsipursky and Drits 1984) from the crystal structures of pyrophyllite (Lee and Guggenheim 1981) and muscovite (Guggenheim et al. 1987). The important adsorptive properties of clays and their environmental applications demand a firm theoretical understanding of their structure and behavior.

The cations of the octahedral sheet are coordinated by six O atoms, two of which involve hydroxyl groups. Most of the properties of these OH groups depend on the nature of the cations bonded to them. The study of the structure and properties of these hydroxyl groups is interesting, because they can play a major role in the crystallographic and physical-chemical properties of these minerals and in their stability and interactions with water, other molecules, and cations.

Some experimental crystallographic features and the thermal behavior of dioctahedral phyllosilicates could not previously be explained with an idealized model of the crystal structure and thus additional considerations were needed to understand the crystal structure. In dioctahedral phyllosilicates, one of the three octahedral positions per asymmetric unit is not occupied by a cation, but instead is a vacant site. Two kinds of configurations exist depending on the disposition of the hydroxyl groups in the octahedral sheet with respect to a vacancy. These OH groups can be on the same side (configuration cis-vacant) or on opposite sides (trans-vacant) with respect to the vacant octahedral site (Fig. 1). The 2:1 layer has a center of symmetry in the trans-vacant configuration but not in the cis-vacant configuration (Tsipursky and Drits 1984). These configurations are not present in the same octahedral sheet, but they may occur in different layers. Hence trans-vacant and cis-vacant forms are polymorphs of these dioctahedral clays. The cis-vacant/trans-vacant proportion can be determined in illite/smectite (I/S) interstratifications by X-ray diffraction and thermal analysis, but only with a semi-quantitative accuracy (Drits et al. 1998). The cis-vacant configuration dehydroxylates at a higher temperature compared to the trans-vacant configuration. However, this does not mean that the cis-vacant configuration is more stable than the trans-vacant configuration, but possible mechanism differences and kinetic effects should

* E-mail: sainz@lec.ugr.es

0003-004X/05/1112–1827$05.00/DOI: 10.2138/am.2005.1819

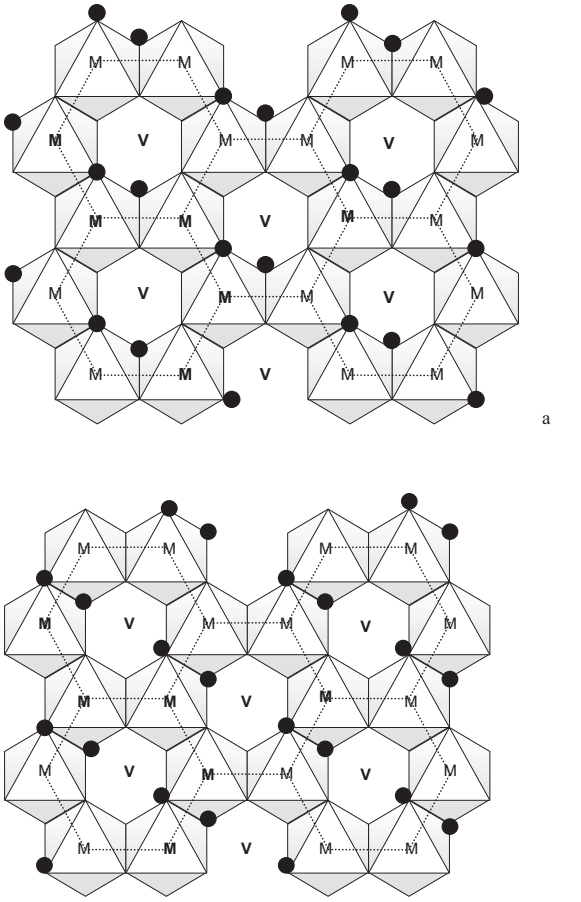

FIGURE 1. Octahedral sheet of cis-vacant (**a**) and trans-vacant (**b**) configurations in dioctahedral 2:1 phyllosilicates. The black circles represent OH groups and M and V are the octahedral centers, occupied cation site and vacant site, respectively.

be considered (Brigatti and Guggenheim 2002). In smectite, the octahedral sheet tends to be cis-vacant, whereas illite has mainly a trans-vacant configuration. During the illitization process of smectite, the formation of illite layers should lead to an increase in the proportion of trans-vacant layers. However, no proportional relationship between the polymorph ratio and the rate of transformation from smectite to illite has been found associated with this process (Cuadros and Altaner 1998; Drits 2003). In addition, the effect of cation substitution on the cis-vacant/trans-vacant ratio remains poorly understood. In fact, discrepancies occur in previous experimental studies. For example, Tsipursky and Drits (1984) found that montmorillonite and Al-rich smectite are cis-vacant, whereas McCarty and Reynolds (1995) discovered that the proportion of cis-vacant layers increased with tetrahedral Al content. One aim of this work is to study these cis-vacant and trans-vacant systems at an atomic scale and the influence of the isomorphous substitution of cations in the octahedral sheet on the crystal structures of both systems.

Atomistic calculations with empirical potentials were performed for 2:1 phyllosilicates in trans-vacant (Liang and Hawthorne 1998; Sainz-Díaz et al. 2001a) and cis-vacant (Sainz-Díaz et al. 2001b) polymorphs with good agreement between the studies and experimentally derived structural data. However, the hydrogen bonds, the relatively weak interactions in the interlayer, and the real total energy calculations require the most sophisticated and exact methods provided by quantum mechanics. In recent years, density functional theory (DFT) with periodic boundary conditions has been used to help understand the behavior and properties of phyllosilicates (Bickmore et al. 2003; Hobbs et al. 1997; Sainz-Díaz et al. 2002) with good agreement with experimental data. This methodology describes the interlayer space with low charge better than do empirical potentials, especially methods based on atomic orbitals. In the present work, this methodology is extended to the study of the trans-vacant and cis-vacant polymorphism for configurations of smectite and illite with differing compositions and cation substitutions. In most cases, we are able to obtain reasonably good agreement with experimental data, and can account for trends in structural features with chemical composition.

MODELS AND METHODS

A series of dioctahedral 2:1 phyllosilicates were studied with different compositions (Table 1) and involving different tetrahedral, octahedral, and interlayer (IC) charges, including smectite (low IC, mainly from the octahedral sheet), and illite (medium and high IC, mainly from the tetrahedral sheet). Different cation substitutions of Si^{4+} by Al^{3+} in the tetrahedral sheet and Al^{3+} by Mg^{2+} and Fe^{3+} in the octahedral sheet were studied, along with several interlayer cations (Na^+ and K^+). Unit cells with periodic conditions were used as starting material. Hence, only specific cation compositions were studied because partial occupancies with this quantum-mechanical methodology are not possible. This fact and the limited size of one unit cell as an asymmetric unit forced us to use models of highly charged smectites and with higher contents of Mg^{2+} or Fe^{3+} than the natural samples. Nevertheless, although some of these compositions are not likely to be found in nature, these models are useful to explore the effect of cation substitutions on cis-vacant and trans-vacant polymorphism in these minerals. In models with two octahedral cation substitutions per unit cell, the cation distribution with lowest energy was chosen (Sainz-Díaz et al. 2002). Then, in samples 6 and 7 with two Mg^{2+} cations, they alternate with the Al^{3+} atom, whereas in sample 3 with two Fe^{3+} cations, they are adjacent to each other and form FeFe pairs. In the samples with one Al^{IV} per unit cell, it is distributed to form a tetrahedral sheet with Al^{IV} or a tetrahedral sheet without Al^{IV}, similar to an interstratified illite(I)/smectite(S) where the tetrahedral sheets follow a alternant sequence with the ordered motif …ISISIS… Sample 9, with two Al^{IV} cations per unit cell, has one Al^{IV} atom in each tetrahedral sheet, and thus, all tetrahedral sheets have Al^{IV}, like a highly charged illite.

In smectite/illite samples, no experimental atom coordinate set is available. Nevertheless, initial geometries were obtained from the models proposed by Tsipursky and Drits (1984) based on oblique-texture electron diffraction studies of dioctahedral smectites. The hydrogen positions were taken from previous studies (Giese 1979) after an optimization performed previously by Sainz-Díaz et al. (2001a).

Total energy calculations were performed using the numerical atomic orbital (NAO) methodology implemented in the SIESTA program (Artacho et al. 1999). This is a method based on DFT that scales linearly with the number of atoms in the simulation cell. The generalized gradient approximation (GGA) and the Perdew-Burke-Ernzerhof (PBE) parameterization (Perdew et al. 1996) of the exchange-correlation functional were used. A uniform mesh with a certain plane-wave cut-off energy was used to represent the electron density, the local part of the pseudopotential, and the Hartree and exchange-correlation potentials. Core electrons were replaced by norm-conserving pseudopotentials (Troullier and Martins 1991) factorized in the Kleinman-Bylander form (Kleinman and Bylander 1982), including scalar-relativistic effects (Bachelet and Schluter 1982). For K and Fe, nonlinear partial-core corrections were added (Louie et al. 1982). The pseudopotentials simulate the interaction between the valence electrons and the cores (nuclei plus core electrons) and neither core electrons nor core wave functions are included explicitly. With this approximation, the valence wave functions are substituted by pseudo-wave functions that do not present strong oscillations in the core region.

TABLE 1. Chemical composition of dioctahedral phyllosilicate samples studied on the unit-cell basis for $O_{20}(OH)_4$ (T = tetrahedral, Oc = octahedral)

Sample	Si^{4+} (T)	Al^{3+} (T)	Al^{3+} (Oc)	Mg^{2+} (Oc)	Fe^{3+} (Oc)	Interlayer cation
1	7	1	4			K^+
2	7	1	3		1	Na^+
3	7	1	2		2	Na^+
4	7	1	4			Na^+
5	8		3	1		Na^+
6	8		2	2		$2Na^+$
7	8		2	2		$2K^+$
8	7	1	3	1		$2Na^+$
9	6	2	4			$2K^+$

The basis sets are made up of strictly localized numerical atomic orbitals (NAOs). Their localization cut-off radii correspond to an energy shift of 270 meV (Artacho et al. 1999). The basis set used in this work is double-Z polarized (DZP) following the perturbative polarization scheme (Artacho et al. 1999). Calculations were restricted to certain values of the number of *k*-points in the irreducible wedge of the Brillouin zone. This number was determined after preliminary calculations (see below). In each structure, the atoms and cell parameters were all relaxed by means of conjugated gradient minimizations with a force tolerance of 0.04 eV/Å as a convergence criterion.

RESULTS AND DISCUSSION

Previous calculations with this methodology on these minerals found that the minimal conditions for accurate results should be with the DZP basis set, and at least 150 Ry of mesh cut-off energy (Sainz-Díaz et al. 2002). In the present work, the calculations were set up to explore different values of mesh cut-off energy and different numbers of *k*-points in the irreducible wedge of the Brillouin zone to optimize the level of the calculations. The higher value of these parameters produces a higher level of the calculations, and thus the computational effort is much greater.

For this preliminary study, we chose a standard sample of illite/smectite (1) with a composition close to that of a potassium beidellite (Table 1). The mesh cut-off energy does not represent the energy of the structure, but it is only a control parameter for improving the level of the calculation (Artacho et al. 1999). A wide range of mesh cut-off energy values was explored by calculating the total energy of the experimental crystal structure and fully optimized structure (Fig. 2a) in the Γ point of the Brillouin zone. With a mesh cut-off energy higher than 100 Ry, the total energy decreases asymptotically with the increase of the cut-off energy, reaching a stability value with cut-off energy values greater than 300 Ry (slope lower than 0.0004 eV/Ry). The total energy calculations of the experimental crystal structures showed the same behavior as the fully optimized structures. This study was extended to samples that contain Fe cations to determine the effect of the presence of this transition metal. Thus, samples 2 (with one Fe cation per unit cell) and 3 (with two Fe^{3+} cations, 50% of the Fe^{3+} in octahedral sheet) were also calculated with different values of mesh cut-off energy. The results showed the same behavior as in sample 1. Therefore, the total energy of our samples can be considered independent of the mesh cut-off energy parameter for values of this parameter greater than 400 Ry.

Another calculation parameter is the number of *k*-points for the sampling of the Brillouin zone. The higher the number of sampling *k*-points involved in the calculation of the wavefunction, the more accurate the electronic structure of the system, but the computational effort is also greater. This is a discrete variable

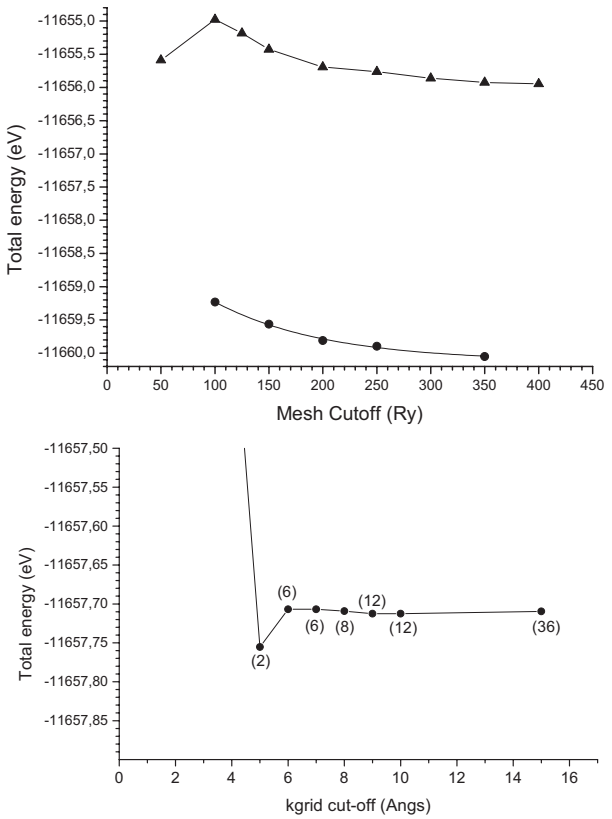

FIGURE 2. Variation of the total energy of sample 1 calculated with different values of Mesh cutoff (**a**), with triangles for experimental geometry and circles for fully optimized structures, and with different *k*-grid cutoff values (**b**) with experimental geometry. The numbers in brackets represent the number of sampling *k*-points corresponding to the *k*-grid cutoff value.

and can be described by a continuous parameter called "*k*-grid cut-off". The *k*-grid cut-off determines the fineness of the *k*-grid used for Brillouin zone sampling. When this parameter is zero, the calculation is on the Γ point in the Brillouin zone. Different values of k-grid cut-off were explored by calculating the total energy of the experimental crystal structure of 1 (Fig. 2b) and fully optimizing this structure with a mesh cut-off energy of 150 Ry. In both cases, a drastic decrease of total energy was found with an increase of k-grid cut-off to obtain a minimum total energy at 5 Å. For higher values of k-grid cut-off, the ΔE is smaller reaching a constant value of total energy at a *k*-grid cut-off of 8 Å (ΔE_{max} < 0.003 eV). This study was extended to single-point calculations of the experimental crystal structure of sample 1 with a mesh cut-off energy of 400 Ry, to check a possible interaction between both parameters (mesh cut-off energy and *k*-grid cut-off). The behavior was identical to former calculations. In addition, the presence of Fe cations was also explored by extending this study to sample 3 (with two Fe cations per unit cell, 50% of the Fe^{3+} in the octahedral sheet). The results showed the same behavior as in sample 1. Hence, the total energy is independent of the *k*-grid cut-off for values of >8 Å in our systems.

The effect of mesh cut-off energy and *k*-grid cut-off on the optimization process was also investigated. The geometric fea-

tures obtained with a mesh cut-off energy of 150 Ry and a k-grid cut-off of 5 Å were close to those obtained from experimental data. Larger values of these parameters did not yield significant differences in geometrical features. From these preliminary calculations, we concluded that our samples could be optimized with a mesh cut-off energy of 150 Ry and a *k*-grid cut-off of 5 Å. However, single point calculations on these optimized structures with a mesh cut-off energy of 500 Ry and a k-grid cut-off of 8 Å were performed for comparative studies of absolute energy values.

CIS-VACANT AND TRANS-VACANT STRUCTURE FORMS

Some of trans-vacant structures were presented previously (Sainz-Díaz et al. 2002) but we have recalculated them with the new optimized conditions obtaining similar geometrical features. Nevertheless we have included them here for comparison between both trans-vacant and cis-vacant polymorphs. Our calculations reproduce the experimental crystal lattice parameters of the illite-smectite series, especially *a*, *b*, *c*, and β for both the trans-vacant and cis-vacant configurations (Tables 2 and 3). The calculated lattice parameters *c* and β are smaller in the cis-vacant configurations than in the trans-vacant structures according to experiment (Drits and McCarty 1996). Both parameters are related to the *d*(001) spacing (*c*.sinβ) and the effects of these values are balanced and the *d*(001) spacing is maintained at similar values for both polymorphs. In some cases the *b* parameter is slightly higher in the cis-vacant form than in the trans-vacant form. No other significant differences were found between the trans-vacant and cis-vacant configurations. The theoretical T-O bond length (T = tetrahedral cation) is slightly longer than the experimental values, a problem that has been traced to the perturbative polarization orbitals of T (Junquera et al. 2001). Nevertheless, the T-O bond length is larger in the samples with Al^{IV}, owing to the larger ionic radius of Al than Si.

The M-O and M-OH distances increase with increasing of Mg^{2+} content, owing to the larger radius of Mg^{2+} compared to Al^{3+}. The corrugation effect of basal oxygen atoms is small in samples 6 and 7. The cation composition of samples 6 and 7 yields a homogeneous distribution of Mg^{2+} in the octahedral sheet and cations in the interlayer that decreases the tilting of the tetrahedra.

No significant differences were observed with the change of interlayer cation (Na^+ for K^+). The *c* parameter is slightly greater in the K^+ samples than in the Na^+ samples, which is probably related to the larger ionic radius of K^+. Nevertheless, the difference in ionic radii between K^+ and Na^+ is greater than the difference in the *c* parameter. This indicates that the K^+cation is more deeply inside the tetrahedral ring cavity than Na^+. This is consistent also with the experimental observation that the presence of K^+ in the interlayer decreases the swelling property of clays (Cuadros and Linares 1996).

Atomic positions of the optimized crystal structures are described in the Supplementary Material for both trans-vacant and cis-vacant polymorphs. We used unit cells (*P*1 symmetry) in our optimizations because the cation substitutions break the symmetry of the initial models of Tsipursky and Drits (1984). The main differences are in the positions of the O and H atoms owing to the changes in the coupling between tetrahedra and octahedra for each configuration. No significant difference was detected in the positions of the Si and Na atoms. These atomic positions are consistent with the models proposed by Tsipursky and Drits (1984).

The powder X-ray diffraction pattern simulations of these optimized structures were performed using the diffraction software in the Cerius2 package with a wavelength of 1.54 Å. The positions and relative intensities of the major reflections are described in Table 4 for samples 3 (trans-vacant) and 4 (trans-vacant and cis-vacant). The reflection positions are similar for each sample; however, some differences occur in relative intensities. The reflections for the calculated structures are in good accord with

TABLE 2. Crystal structure parameters calculated for the cis-vacant (cv) and trans-vacant (tv) configurations of illite-smectites with Na^+ as the interlayer cation (lengths in Å and angles in degrees)

Sample*	Exp †	2_{tv}	2_{cv}	3_{tv}	3_{cv}	4_{tv}	4_{cv}	5_{tv}	5_{cv}	6_{tv}	6_{cv}	8_{tv}	8_{cv}
a	5.18	5.25	5.24	5.25	5.23	5.26	5.25	5.27	5.28	5.26	5.28	5.26	5.27
b	8.97–9.01	9.05	9.08	9.01	9.09	9.07	9.08	9.12	9.10	9.10	9.06	9.12	9.09
c	10.05–10.2	10.07	9.93	10.05	9.92	10.06	9.99	10.08	9.88	9.99	9.98	10.10	10.0
d(001)	9.91–10.0	9.82	9.81	9.77	9.79	9.84	9.87	9.82	9.76	9.79	9.84	9.89	9.88
α	89–91	89.7	91.3	89.7	91.2	89.9	91.4	90.0	91.0	90.0	90.6	90.5	89.7
β	99.5–101.4	102.5	98.9	103.5	99.4	101.9	98.9	103.0	98.9	101.6	99.5	101.8	99.0
γ	89–91	89.8	90.3	89.9	90.2	90.0	90.4	90.0	90.0	90.0	90.0	90.0	90.1
T. th. ‡	2.25§	2.29	2.29	2.29	2.29	2.28	2.28	2.29	2.27	2.33	2.33	2.32	2.32
O. th. ‡	2.11#	2.12	2.12	2.10	2.10	2.13	2.13	2.15	2.17	2.15	2.22	2.15	2.17
Int. th. ‡		3.12	3.12	3.09	3.11	3.15	3.18	3.08	2.97	2.97	2.99	3.09	3.06
Δ*Z*‖		0.34	0.32	0.30	0.33	0.32	0.33	0.32	0.23	0.14	0.14	0.32	0.24
τ‖		109.4	109.4	109.4	109.4	109.4	109.4	109.3	109.4	109.3	109.3	109.3	109.3
O-H ‖	0.95§	0.983	0.983	0.985	0.985	0.979	0.981	0.980	0.980	0.982	0.982	0.979	0.981
T-O‖	1.64§	1.679	1.678	1.678	1.678	1.680	1.679	1.674	1.671	1.682	1.681	1.687	1.686
M-O‖	1.94§	1.960	1.956	1.959	1.950	1.955	1.955	1.991	1.999	2.030	2.033	1.998	1.997
M-OH‖		1.927	1.936	1.936	1.939	1.927	1.931	1.955	1.953	1.988	1.978	1.964	1.958
ε‖		0.414	0.293	0.446	0.310	0.394	0.294	0.429	0.290	0.382	0.312	0.393	0.297

* tv = trans-vacant, cv = cis-vacant, the most stable configuration was chosen in the samples where different cation configurations were possible. In samples 5 and 6 the average values of the two most stable configurations were considered.
† Experimental values for illite/smectites (Tsipursky and Drits 1984).
‡ T. th. = tetrahedral sheet thickness, O. th. = octahedral sheet thickness, Int. th. = interlayer thickness.
§ Experimental data for muscovite (Guggenheim et al. 1987).
# From muscovite (Brigatti and Guggenheim 2002), $(Cl^+)_{0.68}(Al_{1.83}Fe^{3+}_{0.03}Fe^{2+}_{0.04}Mg_{0.1}Mn_{0.04})(Si_{3.51}Al_{0.44})$.
‖ Mean values, Δ*Z* = corrugation effect of basal oxygen surfaces, τ = the O_{basal} - T - O_{apical} bond angle, T is the cation of the tetrahedral sheet, M is the cation of the octahedral sheet, ε = |*c*.cos β|/*a*.

TABLE 3. Crystal-structure parameters calculated for the cis-vacant (cv) and trans-vacant (tv) configurations of illite-smectites with K^+ as the interlayer cation (lengths in Å and angles in degrees)

Sample*	Exp †	1_{tv}	1_{cv}	7_{tv}	7_{cv}	9_{tv}	9_{cv}
a	5.18	5.28	5.26	5.29	5.30	5.28	5.27
b	8.97–9.01	9.12	9.11	9.15	9.12	9.13	9.13
c	10.05–10.2	10.12	10.10	10.07	10.03	10.39	10.36
d(001)	9.91–10.0	9.90	9.98	9.86	9.88	10.17	10.23
α	89–91	89.6	91.1	90.0	90.5	90.0	90.0
β	99.5–101.4	102.1	98.7	101.7	99.9	101.7	99.2
γ	89–91	90.0	90.4	90.0	90.0	90.0	90.0
T. th. ‡	2.25§	2.29	2.28	2.33	2.34		
Oc. th. ‡	2.11#	2.13	2.13	2.14	2.20		
Int. th. ‡		3.19	3.28	3.04	3.03		
ΔZ‖		0.31	0.34	0.15	0.13		
τ‖		109.4	109.4	109.2	109.2		
O-H ‖	0.95§	0.979	0.981	0.982	0.981	0.979	0.979
T-O‖	1.64§	1.677	1.677	1.679	1.678	1.678	1.678
M-O‖	1.94§	1.960	1.957	2.032	2.034	1.958	
M-OH‖		1.934	1.933	1.994	1.989	1.937	1.94
ε‖		0.401	0.290	0.386	0.325	0.399	0.314

* tv = trans-vacant, cv = cis-vacant, the most stable configuration was chosen in the samples where different cation configurations were possible. In sample 7 the average values of the two most stable configurations were considered.
† Experimental values for illite/smectites (Tsipursky and Drits 1984).
‡ T. th. = tetrahedral sheet thickness, O. th. = octahedral sheet thickness, Int. th. = interlayer thickness.
§ Experimental data for muscovite (Guggenheim et al. 1987).
# From muscovite (Brigatti and Guggenheim 2002), $(Cl^+)_{0.68}(Al_{1.83}Fe^{3+}_{0.03}Fe^{2+}_{0.04}Mg_{0.1}Mn_{0.04})(Si_{3.51}Al_{0.44})$.
‖ Mean values, ΔZ = corrugation effect of basal oxygen surfaces, τ = the O_{basal}-T-O_{apical} bond angle, T is the cation of the tetrahedral sheet, M is the cation of the octahedral sheet, $\varepsilon = |c.\cos\beta|/a$.

TABLE 4. Main XRD reflections from the simulated powder XRD pattern of the optimized structures of samples 3 (trans-vacant), 4 (trans-vacant), and 4 (cis-vacant)

hkl		*d*-spacing (Å)			Relative intensity (%)		
	Exp. *	3-trans	4-trans	4-cis	3-trans	4-trans	4-cis
001	9.98, 10.1	9.781	9.842	9.864	100.0	100.0	100.0
002	4.98	4.890	4.921	4.932	2.9	33.8	33.8
020	4.48†, 4.50	4.509	4.535	4.539	48.2	94.6	21.7
1$\bar{1}$0		4.437	4.476	4.525	0.3	1.9	54.2
110		4.448	4.479	4.483	0.3	2.8	53.3
11$\bar{1}$	4.35	4.391	4.382	4.327	18.5	36.8	10.4
111		4.400	4.382	4.317	19.1	40.6	9.1
02$\bar{1}$		4.079	4.117	4.165	1.6	1.6	12.8
11$\bar{1}$		3.757	3.824	3.936	2.4	0.9	12.0
11$\bar{2}$		3.691	3.654	3.557	17.9	27.5	4.4
112	3.65	3.674	3.652	3.589	19.5	33.0	6.1
022		3.298	3.332	3.384	0.6	4.7	27.9
022	3.33‡	3.332	3.337	3.297	1.1	5.6	26.4
003	3.32	3.260	3.281	3.288	41.1	65.5	60.4
112		2.990	3.050	3.149	16.3	33.9	13.4
112	3.07	3.006	3.052	3.099	16.9	33.1	15.1
113		2.921	2.905	2.859	1.3	6.0	20.4
113		2.935	2.907	2.829	1.4	6.7	18.2
023	2.67	2.655	2.660	2.630	7.4	12.6	4.0
023		2.629	2.656	2.697	7.6	12.6	6.2
200	2.57†	2.552	2.574	2.594	15.2	21.4	24.2
131	2.57§	2.5785	2.588	2.580	15.5	25.1	19.8
13$\bar{1}$		2.584	2.588	2.573	15.3	26.4	23.1
131		2.426	2.456	2.504	2.9	17.9	17.6
202	2.52†	2.517	2.502	2.457	4.7	17.1	15.5
131	2.47	2.442	2.459	2.456	3.2	16.5	14.6
132	2.405§	2.404	2.409	2.402	9.2	12.6	14.1
132		2.417	2.411	2.373	9.3	11.8	14.1
201		2.339	2.374	2.418	10.5	17.4	11.8
005	1.99	1.956	1.968	1.973	4.2	16.1	15.4
331		1.509	1.516	1.519	8.1	16.4	14.7
060	1.50 *†	1.503	1.512	1.513	8.5	16.2	15.2

* In illite (Brindley and Brown 1980) except for the cases indicated.
† In beidellite (Brindley and Brown 1980).
‡ In micas (Drits 2003).
§ In muscovites (Brindley and Brown 1980).

experimental data reported previously for illite, beidellite, and muscovite (Brindley and Brown 1980). In all of the samples the most intense reflection is 001. However, in sample 3 the rest of the reflections have much lower relative intensity than in sample 4. This difference is explained by the lower symmetry produced by the substitution of Al^{3+} by Fe^{3+}. In the trans-vacant form, the main reflections follow the intensity sequence 001 > 020 > 003, whereas in the cis-vacant form this sequence is 001 > 003 > 1$\bar{1}$0 > 110. The 002 reflection of the trans-vacant form (sample 3) has a significantly lower intensity than in sample 4. This is consistent with the observation that the 002 intensity decreases with increasing Fe^{3+} content in the octahedral sheet (Brindley and Brown 1980). The 060 reflection appears in all samples at 1.50–1.51 Å, which is a characteristic of dioctahedral clays (1.50 Å), whereas in trioctahedral clays this reflection appears at 1.53–1.55 Å (Brindley and Brown 1980).

The simulated powder X-ray diffraction patterns based upon the theoretical structure agrees with the experimental peak positions of the main reflections (Reynolds 1993), although experimental high resolution XRD patterns are difficult to locate because of the high level of disorder (composition, cation substitution, layer stacking, etc.) of most samples. In Figure 3, powder XRD patterns simulated from the calculated crystal structure are presented and the cis-vacant and trans-vacant forms are compared in Figure 4 for a particle size of 50 nm (Fig. 4a). Small differences are observed with regard to position differences and the absence of some reflections. Thus, the 110 reflection can be distinguished in the cis-vacant form but not in the trans-vacant form. The 11$\bar{1}$, 112, and 201 reflections show different positions and intensities between the cis-vacant and trans-vacant forms. The 111 reflection is more intense in the cis-vacant form and appears at lower 2θ units than in the trans-vacant form. In contrast, the 11$\bar{2}$ and 11$\bar{1}$ reflections are more intense in the trans-vacant form and appear at a slightly lower 2θ values than in the cis-vacant form. The 112 reflection of the trans-vacant form is more intense and appears at higher 2θ than in the cis-vacant form. The 020 reflection appears in the same position for both polymorphs, however the differences in 2θ between the 020 and 11$\bar{1}$ reflections is slightly greater in the cis-vacant form than in the trans-vacant form. These differences are more easily detected in these ideal theoretical crystal structures; it is difficult to distinguish them experimentally. This differentiation will be more difficult in fractions with small particle sizes (20 nm) that can be present in clays. Simulating the powder XRD trace of our calculated samples for this particle size of 20 nm, a broadening of the peaks is observed and the differences in the powder XRD patterns between both polymorphs are more difficult to observe and to quantify accurately (Fig. 4b). Nevertheless, most of the differences between the calculated patterns for the cis and trans forms are consistent with experiment. The 02$\bar{1}$, 021, 1$\bar{1}$1, 111, 11$\bar{3}$, and 1$\bar{1}$3 reflections can be observed clearly in the cis-vacant forms even in the 20 nm fractions, whereas they are not intense in the trans-vacant forms. On the contrary, the 11$\bar{2}$ and 112 reflections are much more intense in the trans-vacant forms than in the cis-vacant forms. These differences match those found experimentally by Drits (2003) in cis and trans mixtures of 1*M* micas. This result suggests the validity of the theoretical approach, thereby making it a useful tool for better understanding

experimental results.

The proportion of cis-vacant and trans-vacant layers can be determined by means of the parameter ε (ε = |*c*.cos β |/*a*). This can be calculated from the *d* values of the XRD reflection lines, and it is a statistically weighted sum of the values for each configuration of cis- or trans-vacant forms (for a random interstratification of cis- and trans-vacant layers). In the fitting procedure for the quantitative determination of cis/trans proportions from XRD patterns, the values of ε must be determined for pure cis-vacant or trans-vacant configurations. However, different experimental values have been reported for similar samples, such as ε_{cis} = 0.308 and ε_{trans} = 0.383 (McCarty and Reynolds 1995) and ε_{cis} = 0.302 and ε_{trans} = 0.400 (Drits and McCarty 1996), making it difficult to apply the procedure to other samples. Our calculations permit us to determine these values for pure cis-vacant and pure trans-vacant layers for different cation compositions. Thus, considering all our samples, the average values of ε for the pure cis-vacant and pure trans-vacant configurations are 0.303 and 0.404, respectively. These values are consistent with the data obtained experimentally by Drits and McCarty (1996), confirming the applicability of these values to other clay minerals. Nevertheless, these theoretical averaged values of ε are slightly different, higher in trans forms and lower in cis forms, than the experimental values, owing to the contribution of samples with octahedral compositions unusual for smectite or illite with 50% Fe^{3+} (sample 3, where ε_{tv} is high) or 50% Mg^{2+} (samples 6 and 7, where ε_{cv} is low). Hence, these ε values depend on the cation composition found experimentally (Drits 2003). This is another useful application of the theoretical approach, because for a specific cation composition, these calculations can determine the ε values for pure cis-vacant and trans-vacant forms. Such information is useful for quantitative determinations of the cis-vacant/trans-vacant ratio in experimental XRD studies.

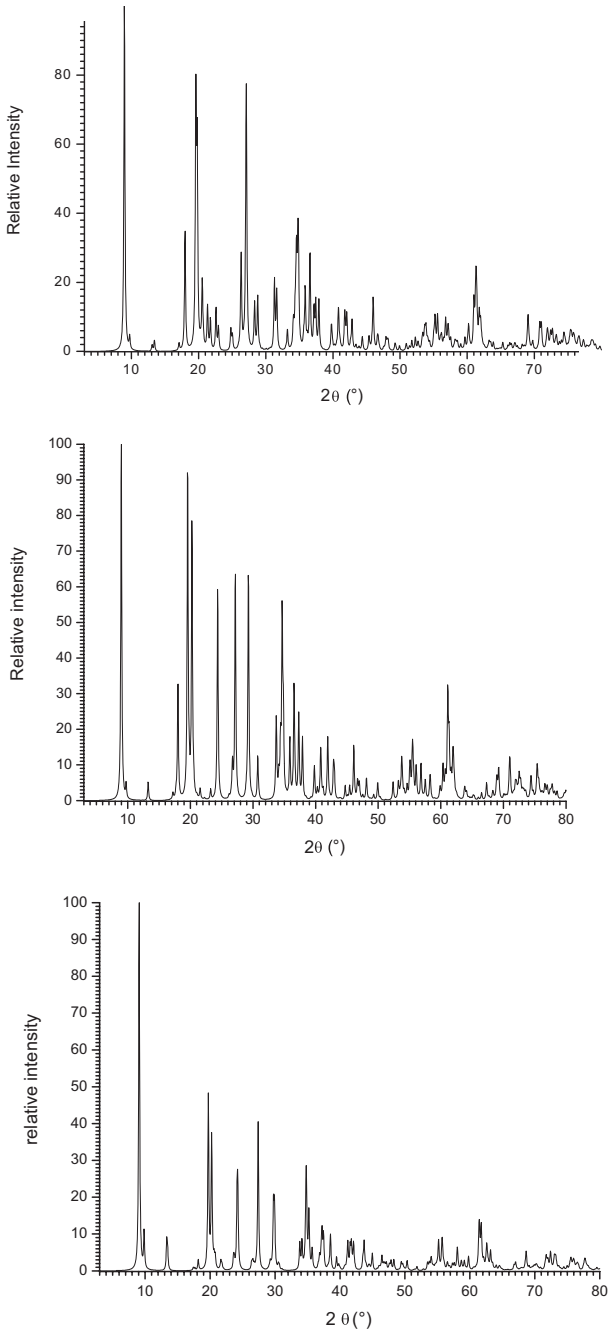

FIGURE 3. Simulated powder X-ray diffraction patterns of the optimized structures: (**a**) cis-vacant and (**b**) trans-vacant polymorphs of sample 4, and (**c**) the trans-vacant form of sample 3.

For the same composition, the energy difference between the cis-vacant and trans-vacant configurations is very small. In Table 5, the energy of the equivalent cation distribution for both polymorphs is compared. Based on our calculations, in beidellite samples 1 and 4, both polymorphs are energetically similar, because the energy difference between them is negligible. Thermodynamically, both polymorphs are equally probable to occur. With cation substitution of Mg^{2+} and Fe^{3+}, the cis-vacant form has a slightly lower energy than the trans-vacant form, except in samples 5 and 7, where the trans-vacant form is slightly more stable than the cis-vacant form. Samples 1–4 and 8 have Al^{IV} in only one tetrahedral sheet adjacent to the interlayer space per unit cell, representing an illite/smectite (I/S) interstratification. On the other hand, sample 9 has a greater tetrahedral charge with Al^{IV} in all tetrahedral sheets, thereby representing an illite structure with a high charge. In the latter sample, the trans-vacant form is more stable than the cis-vacant form. This is consistent with experimental behavior, where illites tend to adopt the trans-vacant form and smectites often form the cis-vacant structure. In all cases, the energy differences between trans-vacant and cis-vacant forms are lower than those obtained from octahedral cation ordering (Sainz-Díaz et al. 2002). Further research explor-

TABLE 5. Energy (ev) differences between the trans-vacant and cis-vacant polymorphs

Sample	*E* (trans-vacant)	*E* (cis-vacant)	Δ*E*(ev) = *E*cis-*E*trans
1	−11661.3518	−11661.3597	−0.0079
2	−12320.8110	−12320.8547	−0.0437
3	−13040.8007	−13040.9614	−0.1607
4	−11601.0766	−11601.0782	−0.0016
5	−11616.9808	−11616.9583	0.0225
6	−11591.6627	−11591.6839	−0.0212
7	−11712.5150	−11712.5082	0.0068
8	−11575.6536	−11575.6931	−0.0395
9	−11680.4678	−11680.3698	0.0980

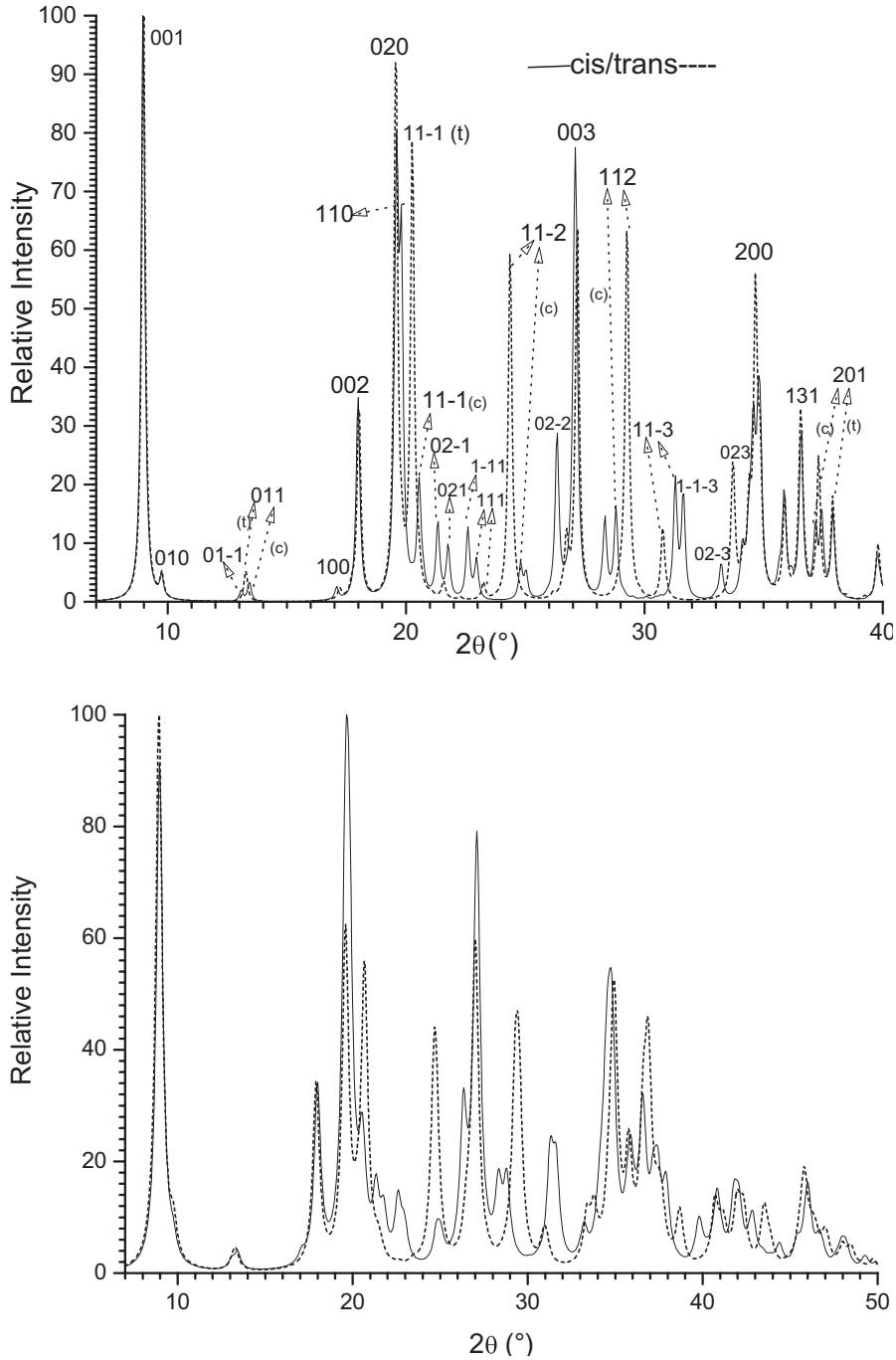

FIGURE 4. Simulated powder X-ray diffraction patterns of the optimized structures: cis-vacant (solid line) and trans-vacant (dashed-line) polymorphs of sample 4, for a particle size of (**a**) 50 nm and (**b**) 20 nm.

ing more realistic cation compositions with larger supercells will be forthcoming.

The low-energy differences found between the polymorphs justifies the non-linear correlation between the illite/smectite proportion and trans-vacant/cis-vacant ratio found experimentally in natural samples (Cuadros and Altaner 1998). Thus, no predictive correlation can be obtained either experimentally or theoretically about the direct effect of cation substitution on the cis-vacant/trans-vacant proportion. Many external factors can affect the cis-vacant to trans-vacant transformation and hence the cis-vacant/trans-vacant ratio in clay minerals. Smectite and illite minerals from the same deposit with very similar chemical compositions may have different cis-vacant/trans-vacant ratios (Tsipursky and Drits 1984; Drits 2003). Such differences were

explained previously by the different physical conditions that occurred during illitization. Variations in conditions may be responsible for mechanisms involving dissolution/precipitation and solid-phase transformations. In general, the proportion of cis-vacant layers decreases with the increase of illite content in interstratifications of illite/smectite samples (Drits et al. 1996; Cuadros and Altaner 1998), but no direct correlation has been found. This cis-vacant to trans-vacant transformation during illitization is more rapid in a dissolution-recrystallization process, whereas in solid-phase illitization the cis-vacant to trans-vacant change is much slower (Drits 2003). In hydrothermal processes, multiple stages of nucleation and crystal growth can be involved, and both trans-vacant and cis-vacant layers can grow simultaneously during the formation of I/S interstratification. Cis-vacant smectites are formed in the initial stages of the degradation of rhyolitic volcanoclastic rocks (Drits 2003). In contrast, trans-vacant I/S samples are formed during the weathering of illite (Drits 2003). Therefore, the different proportion of these polymorphs in natural samples can be explained mainly by kinetic processes during crystal growth and not only by thermodynamic control. Nevertheless, cis-vacant and trans-vacant polymorphism should be considered in further theoretical and experimental studies, in spite of the low energy differences. This polymorphism can explain physical-chemical differences in spectroscopy, X-ray diffraction, crystal growth, and reactivity of clay minerals.

Therefore, this quantum mechanical approach can be a useful tool for the study of polymorphism, especially in those cases where is difficult to distinguish the polymorphs by X-ray diffraction or to analyze them experimentally.

ACKNOWLEDGMENTS

The authors are thankful to E. Artacho for fruitful discussions, to S. Guggenheim for comments and reviewing, and also to the "Centro Técnico de Informática" of CSIC and the "Centro de Supercomputación de la Universidad de Granada" for allowing the use of their computational facilities. E. Escamilla-Roa thanks AECI and the University of Granada and a BTE2000-1146-CO2-01 grant for financial support. This work was also supported by MCYT grants PPQ2001-2932 and BTE2002-03838.

REFERENCES CITED

Artacho, E., Sánchez-Portal, D., Ordejón, P., García, A., and Soler, J.M. (1999) Linear-scaling ab-initio calculations for large and complex systems. Physic Status Solidi, 215, 809–817.

Bachelet, G.B. and Schluter, M. (1982) Relativistic norm-conserving pseudopotentials. Physics Reviews B, 25, 2103–2108.

Bickmore, B.R., Rosso, K.M., Nagy, K.L., Cygan, R.T., and Tadanier, C.J. (2003) Ab initio determination of edge surface structures for dioctahedral 2:1 phyllosilicates: Implicactions for acid-base reactivity. Clays and Clay Minerals, 51, 359–371.

Brigatti, M.F. and Guggenheim, S. (2002) Mica crystal chemistry and influence of P-T-X on atomistic models. In A. Mottana, F.P. Sassi, J.B. Thompson, Jr., and S. Guggenheim, Eds., Micas: Crystal Chemistry and Metamorphic Petrology, 46, 10–85. Reviews in Mineralogy and Geochemistry, Mineralogical Society of America, Chantilly, Virginia.

Brindley, G.W. and Brown, G., Eds. (1980) Crystal Structures of Clay Minerals and their X-ray Identification. Mineralogical Society, London.

Cuadros, J. and Altaner, S.P. (1998) Compositional and structural features of the octahedral sheet in mixed-layer illite/smectite from bentonites. European Journal of Mineralogy, 10, 111–124.

Cuadros, J. and Linares, J. (1996) Experimental kinetic study of the smectite-to-illite transformation. Geochimica and Cosmochimica Acta, 60, 439–453.

Drits, V.A. (2003) Structural and chemical heterogeneity of layer silicates and clay minerals. Clay Minerals, 38, 403–432.

Drits, V.A. and McCarty, D.K. (1996) The nature of diffraction effects from illite and illite-smectite consisting of interstratified trans-vacant and cis-vacant 2:1 layers: a semiquantitative technique for determination of layer-type content. American Mineralogist, 81, 852–863.

Drits, V.A., Lindgreen, H., Salyn, A.L., Ylagan, R., and McCarty, D.K. (1998) Semiquantitative determination of trans-vacant and cis-vacant 2:1 layers in illites and illite-smectites by thermal analysis and X-ray diffraction. American Mineralogist, 83, 1188–1198.

Giese, R.F. (1979) Hydroxyl orientations in 2:1 phyllosilicates. Clays and Clay Minerals, 27, 213–223.

Guggenheim, S., Chang,Y.-H., and Koster van Gross, A.F. (1987) Muscovite dehydroxylation: high-temperature studies. American Mineralogist, 72, 537–550.

Hobbs, J.D., Cygan, R.T., Nagy, K.L., Schultz, P.A., and Sears, M.P. (1997) All-atom ab initio energy minimization of the kaolinite crystal structure. American Mineralogist, 82, 657–662.

Junquera, J., Paz, O., Sánchez-Portal, D., and Artacho, E. (2001) Numerical atomic orbitals for linear-scaling calculations. Physics Reviews B, 64, 235111.

Kleinman, L. and Bylander, D.M. (1982) Efficacious form for model pseudopotentials. Physics Reviews Letters, 48, 1425–1428.

Lee, J.H. and Guggenheim S. (1981) Single crystal X-ray refinement of pyrophyllite-1*Tc*. American Mineralogist, 66, 350–357.

Liang, J.J. and Hawthorne, F.C. (1998) Calculated H-atom positions in micas and clay minerals. Canadian Mineralogist, 36, 1577–1585.

Louie, S.G., Froyen, S., and Cohen, M.L. (1982) Nonlinear ionic pseudopotentials in spin-density-functional calculations. Physics Reviews B, 26, 1738–1742.

McCarty, D.K. and Reynolds, R.C. (1995) Rotationally disordered illite-smectite in paleozoic K-bentonites. Clays and Clay Minerals, 43, 271–284.

Perdew, J.P., Burke, K., and Ernzerhof, M. (1996) Generalized gradient approximation made simple. Physics Review Letters, 77, 3865.

Reynolds, R.C. Jr. (1993) Three-dimensional X-ray powder diffraction from disordered illite: Simulation and interpretation of the diffraction patterns. In R.C. Reynolds Jr. and J.R. Walker, Eds., Computer applications to X-ray powder diffraction analysis of clay minerals, 5, 43–78. The Clay Minerals Society, Boulder, Colorado.

Sainz-Díaz, C.I., Hernández-Laguna, A., and Dove, M.T. (2001a) Modelling of dioctahedral 2:1 phyllosilicates by means of transferable empirical potentials. Physics and Chemistry of Minerals, 28, 130–141.

——— (2001b) Theoretical modelling of cis-vacant and trans-vacant configurations in the octahedral sheet of illites and smectites. Physics and Chemistry of Minerals, 28, 322–331.

Sainz-Díaz, C.I., Timón, V., Botella, V., Artacho, E., and Hernández-Laguna, A. (2002) Quantum mechanical calculations of dioctahedral 2:1 phyllosilicates: Effect of octahedral cation distribution in pyrophyllite, illite, and smectite. American Mineralogist, 87, 958–865.

Troullier, N. and Martins, J.L. (1991) Efficient pseudopotentials in spin-density-functional calculations. Physical Reviews B, 43, 1993–2006.

Tsipursky, S.I. and Drits, V.A. (1984) The distribution of octahedral cations in the 2:1 layers of dioctahedral smectites studied by oblique-texture electron diffraction. Clay Minerals, 19, 177–193.

MANUSCRIPT RECEIVED SEPTEMBER 20, 2004
MANUSCRIPT ACCEPTED MARCH 20, 2005
MANUSCRIPT HANDLED BY STEPHEN GUGGENHEIM